Structure−Kinetic Relationships of Passive Membrane Permeation from Multiscale Modeling

Callum J. Dickson,* Viktor Hornak, Robert A. Pearlstein, and Jose S. Duca

Computer-Aided Drug Discovery, Global Discovery Chemistry, Novartis Institutes for BioMedical Research, 181 Massachusetts Avenue, Cambridge, Massachusetts 02139, United States

S Supporting Information

ABSTRACT: Passive membrane permeation of small molecules is essential to achieve the required absorption, distribution, metabolism, and excretion (ADME) profiles of drug candidates, in particular intestinal absorption and transport across the blood−brain barrier. Computational investigations of this process typically involve either building QSAR models or performing free energy calculations of the permeation event. Although insightful, these methods rarely bridge the gap between computation and experiment in a quantitative manner, and identifying structural insights to apply toward the design of compounds with improved permeability can be difficult. In this work, we combine molecular dynamics simulations capturing the kinetic steps of permeation at the atomistic level with a dynamic mechanistic model describing permeation at the in vitro level, finding a high level of agreement with experimental permeation measurements. Calculation of the kinetic rate constants determining each step in the permeation event allows derivation of structure−kinetic relationships of permeation. We use these relationships to probe the structural determinants of membrane permeation, finding that the desolvation/loss of hydrogen bonding required to leave the membrane partitioned position controls the membrane flip-flop rate, whereas membrane partitioning determines the rate of leaving the membrane.
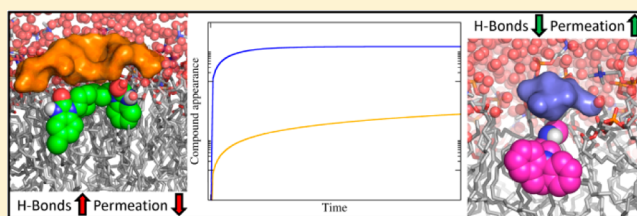
INTRODUCTION

Transport of small molecules across biomembranes is a fundamentally important mechanism to achieve suitable bioavailabilty or intracellular exposure. It is also essential to crossing the blood−brain barrier for molecules unable to appropriate an active transport mechanism. While active transport processes exist for endogenous hydrophilic substances such as sugars and amino acids, the predominant mechanism by which xenobiotics cross membranes is through permeation across the lipid bilayer along a concentration gradient.[1] A thorough understanding of passive membrane permeation is therefore required to efficiently optimize ADME-Tox properties during drug discovery and development.[2,3] Furthermore, the development of ligands targeting membrane proteins may benefit from such knowledge, given that certain drugs may enter the binding site via the membrane or may modulate membrane proteins allosterically by binding to an external membrane-exposed site.[4,5]

Historically, Overton's rule has been used to predict passive membrane transport, whereby molecules with a higher oil/water partition coefficient (log P) are predicted to have faster membrane permeation.[6] This observation allowed the development of the solubility-diffusion model for membrane permeation, whereby the membrane is treated as a homogeneous solvent and movement is determined by Fick's law of diffusion.[7] However, studies of lipid bilayers, a simple representation of the full cell membrane, have revealed a more complex heterogeneous picture than an oily slab, given

that lipids contain polar head groups and nonpolar chains.[8] To account for this, the inhomogeneous solubility-diffusion model was developed,[9,10] taking into account depth-dependent partitioning, resistance, and diffusion parameters. These models assume that diffusion through a single membrane barrier is the rate-limiting step; therefore, resulting permeation profiles are monoexponential.[11] However, for lipophilic compounds, the membrane may act as both a barrier and a sink,[12] meaning that desorption from the membrane into the acceptor compartment may be the rate-limiting step in overall permeation. Permeation of lipophilic drug-like molecules may therefore require a different theoretical treatment.

A limited number of studies investigating membrane permeation have used a kinetic model to better capture the processes involved in crossing a lipid bilayer.[11,13−19] The overall rate of permeation depends on the kinetic rate constants (and respective reverse rate constants) of three consecutive steps involved in such dynamic models of permeation:

1. Membrane entry (partitioning).
2. Flip-flop across the hydrophobic membrane core.
3. Membrane exit.

Such a model is depicted in Figure 1. If the small molecule is charged, then it first becomes protonated/deprotonated depending on the pK_a value of the molecule. It then partitions into the membrane with rate constant k_{in} (and may leave the
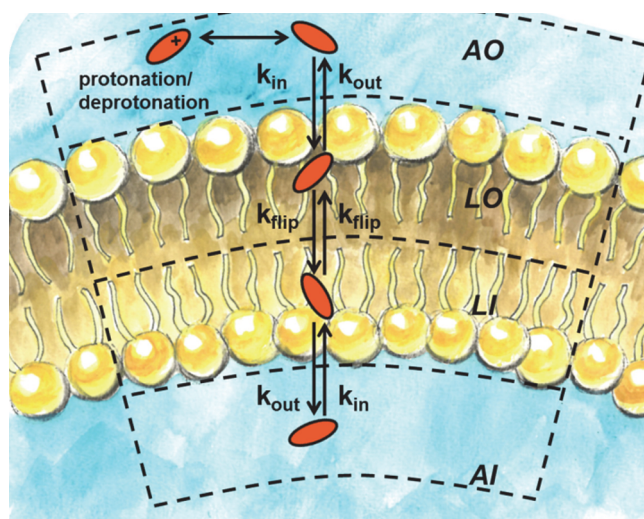
Figure 1. Kinetic model of small molecule membrane permeation involving four compartments. The small molecule substrate approaches the membrane from the aqueous outer phase (AO) which has volume V_{AO}, becoming protonated/deprotonated depending on charge state. The small molecule then moves across the membrane head groups with rate constant k_{in} (membrane has surface area A_{LO}) to partition into the outer membrane layer, LO, which has volume V_{LO}. Flip-flop across the membrane hydrophobic core then proceeds with rate constant k_{flip}, allowing the molecule to move into membrane inner layer, LI, which has volume V_{LI}. Finally, the small molecule leaves the inner membrane layer to the aqueous inner phase, AI, with rate constant k_{out}, where the AI phase has volume V_{AI}. A full membrane permeation event involves each sequential step.

membrane at rate constant k_{out}), with the ratio of the k_{in} and k_{out} rate constants determining the water/membrane partitioning of the compound. Small amphiphilic drug molecules typically position in the membrane just below the lipid headgroup region.[20] Note that since this position is proton accessible the protonation/deprotonation step may also occur here. The next step is the flip-flop of the molecule across the hydrophobic membrane core, with rate constant k_{flip}. Finally, to undergo a full permeation event, the molecule must exit the headgroup region on the opposite side of the membrane into solvent with rate constant k_{out}. Movement across a membrane is therefore split into a number of steps, meaning that such a model may better describe the bi- or triexponential permeation profiles as observed experimentally.[11]

As overall permeation depends on the respective kinetic rate constants of each sequential step, any single rate constant, or combination of rate constants, may be rate-limiting to permeation. For highly polar molecules, the k_{in} and k_{flip} rate constants determine overall permeation, which is likely to be slow. As lipophilicity increases, k_{in} becomes high, and at certain lipophilicity, k_{flip} and k_{out} may become roughly equivalent and optimal permeation is achieved. At even higher lipophilicity, k_{out} becomes low and limits overall permeation. Consequently, a parabolic relationship between log P and permeation may be observed.[21] To fully investigate permeation with such a model, we require the value of each kinetic rate constant.

Recently, Eyer et al. determined the rate of permeation for a series of seven basic drug compounds using a liposomal fluorescence assay.[22] Given the high accuracy of such a method and the use of a single layer POPC liposome, we can be confident that the measured permeation rate is due solely to passive permeation through the POPC membrane, which may not be the case for Caco-2 or MDCK cell permeation assays.

	Domperidone	Labetalol	Loperamide	Verapamil
Log(Perm$_N$ /[cm s^{-1}])	-2.6	-2.1	-0.42	0.01
pK$_a$	7.9	7.4, 9.4	8.7	8.9
logP	3.9	3.09	5.5	3.79

	Propranolol	Chlorpromazine	Desipramine
Log(Perm$_N$ /[cm s^{-1}])	0.19	0.59	0.65
pK$_a$	9.5	9.3	10.2
logP	3.48	5.41	4.9

Figure 2. Molecular structures, experimental pK_a and log P values, and liposomal permeation rates for the neutral form of seven weakly basic small molecules.[22,49]

Although the membrane composition is closer to the in vivo picture, Caco-2 and MDCK permeation assays involve cell monolayers, and true passive permeation may be obscured by the presence of efflux pumps, the possibility of para-cellular transport, and the unstirred water layer limiting diffusion to the membrane.

Using a liposomal system, Eyer et al. report that neither diffusion in the aqueous layer nor membrane partitioning is rate-limiting to membrane permeation, by determining permeation at different aqueous volume to liposome surface area ratios. We can therefore assume that, for these compounds at least, k_{in} is almost instantaneous on the experimental time scale. Note that this experimental method captures only the permeation of the neutral form of ionic species, consistent with the pH-piston hypothesis[23] and the model depicted in Figure 1.

Detailed computational investigations of permeation in recent years have primarily used molecular dynamics (MD) and the potential of mean force (PMF) method, from which a permeability coefficient may be derived using the inhomogeneous solubility-diffusion model (ISDM).[9,10,24−34] The ISDM appears to capture the permeation of water and other small solutes;[10,27,28,35] however, extension to larger drug-like molecules has given varied results.[32] To investigate the movement of larger solutes across the membrane, techniques such as metadynamics and milestoning add further dimensions to the calculation of membrane permeation from free energy simulations.[12,36−42] Certain studies have investigated the kinetic rates of membrane interaction, such as adsorption to a bilayer surface[43] or flip-flop across the membrane hydrophobic core.[44−47]

In this work, we apply the ISDM to the data set reported by Eyer et al., finding reasonable agreement with experiment. We next combine information from the PMF simulations with short unbiased "downhill" MD simulations to estimate the kinetic rate constants of membrane entry (k_{in}), membrane exit (k_{out}), and flip-flop (k_{flip}) using a Markov state model.[48] By incorporating these rate constant values into a dynamic mechanistic model of liposome permeation, we achieve a higher level of agreement with experiment for permeability coefficients, validating the MD-derived rate constants and indicating that the dynamic model better represents the experimental system than the ISDM. We then use the kinetic rate constants to examine each step in the permeation process and build structure−kinetic relationships of membrane permeation. We find that in order to optimize the two slowest steps in the overall process, k_{flip} and k_{out}, we must balance the enthalpy cost to flip-flop with compound membrane partitioning, which typically tracks with log P.

■ METHODS

Experimental Measurement of Permeation. The data set of seven weakly basic compounds is given in Figure 2, along with pK_a, log P, and liposomal permeation values. Permeation was measured by Eyer et al. using a liposomal fluorescence assay.[22] This assay tracks compound appearance within liposomes using a pH-sensitive fluorophore; proton release by the basic small molecule occurs prior to membrane permeation, and proton uptake within the liposome occurs after permeation. The fluorescence increase over time is fitted to a biexponential function, allowing calculation of apparent permeability coefficients, Perm$_{app}$, which may be converted into permeation coefficients of the neutral form only (Perm$_N$) using the Henderson−Hasselbalch equation. The extrapolation from the

observed Perm$_{app}$ to Perm$_N$ assumes that only the neutral form of the basic compounds permeate. On the basis of the log P and permeability data in Figure 2, it can be seen that for this data set log P is a poor predictor of permeation ($r^2 = 0.27$).

Potential of Mean Force Simulations. The free energy of transfer from the water phase to the center of a POPC membrane was calculated for the seven drug molecules in Figure 2 in neutral form using the umbrella restraint potential of mean force method. Compounds were modeled with the parm@Frosst force field,[50] a small molecule force field that extends AMBER ff99SB,[51] and conformationally averaged AM1-BCC charges;[52−55] lipids were modeled using the AMBER Lipid14 force field[56−58] and water using the TIP3P model.[59] Molecular dynamics simulations were run with AMBER 16[60] and PMEMD CUDA[61−63] on GPU cards.

To obtain starting structures, each drug molecule was placed at the center of an equilibrated 72 POPC membrane with 60 waters per lipid. The system was then energy minimized for 10 000 steps, of which the first 5000 steps used the steepest descent method and the remaining steps used the conjugate gradient method.[64] Initial heating from 0 to 100 K was then applied using Langevin dynamics[65] within a 5 ps constant volume run, with restraints on the drug molecule and lipids (force constant 10 kcal/mol/Å^2). The volume was then allowed to change freely, the temperature was increased to 303 K with a Langevin collision frequency of $\gamma = 1$ ps^{-1}, and anisotropic Berendsen control of the pressure[66] around 1 atm was applied by coupling the periodic box with a time constant of 2 ps for 100 ps. The same restraint of 10 kcal/mol/Å^2 was maintained on the drug compound and lipid molecules.

The pressure relaxation time was then reduced to 1 ps, restraints were removed on lipids, and the system was left to equilibrate for 5 ns in NPT. Three dimensional periodic boundary conditions with the usual minimum image convention were employed. Bonds involving hydrogen were constrained using the SHAKE algorithm,[67] allowing a 2 fs time step. PME was used to treat all electrostatic interactions[68] beyond a cutoff of 10 Å. A long-range analytical dispersion correction was applied to energy and pressure. A harmonic restraint of 2.5 kcal/mol/Å^2 was applied on the drug molecule only, allowing it to move in the x- and y-dimensions but restraining it in the z-dimension.

Drug molecules were then pulled from $z = 0$ Å out to 40 Å (in the bulk water phase) using a pulling rate of 1 Å/ns and force constant of 1.1 kcal/mol/Å^2. The pulling simulation therefore lasted 40 ns and was performed in the NPT ensemble with semi-isotropic pressure scaling. Pulling from the membrane center outward has been shown to increase convergence of final free energy profiles.[69] Snapshots were then saved with the drug molecule positioned at $z = 0$ Å, 1 Å, 2 Å, ..., 40 Å from the membrane center. Each of the 40 windows was then run for 20 ns to allow equilibration, followed by an 80 ns production run, with the ligand restrained in the z-dimension only using a harmonic force constant of 2.5 kcal/mol/Å^2. Trajectory frames were recorded every 10 ps, and drug molecule z-position, every simulation step. The free energy of transfer profile (water → membrane) was then constructed using the weighted histogram analysis (WHAM) program[70] with tolerance of 1×10^{-8} under the assumption that results from the single leaflet were applicable to the opposing leaflet by symmetry. Convergence of each PMF was achieved by an 80 ns run time (see Supporting Information section 1). In order to obtain error estimates, the pulling step was repeated for each

molecule from a different orientation within the membrane core, allowing different snapshots at each position into the membrane to be selected, and the full PMF calculation was repeated (20 ns equilibration and 80 ns production). Final results are therefore the average of independent runs ± standard deviation. One of the seven compounds, verapamil, showed high variance in free energy at the membrane center; a third independent repeat was therefore performed for this molecule. From the PMF results, the position-dependent diffusion, resistance, and overall permeation coefficient was then determined using the inhomogeneous solubility-diffusion model.[9,10,71]

The position-dependent diffusion values were calculated as

$$D(z) = \frac{\mathrm{var}(z)^2}{\int_0^\infty C_{zz}(t)\,\mathrm{d}t} \tag{1}$$

where $C_{zz}(t) = \langle \delta z(0)\, \delta z(t) \rangle$ is the autocorrelation function of the z-position of the drug molecule during the PMF window.[71] This was determined for 1 ns blocks of the production runs (80 blocks total) by integrating the $C_{zz}(t)$ curve until it had decayed to $0.01 \times \mathrm{var}(z)$ such that noise around $C_{zz}(t) = 0$ was discarded from the integration. The $D(z)$ values are therefore averages over 80 estimates.

The position-dependent resistance values are then

$$R(z) = \frac{\exp(\beta \Delta G(z))}{D(z)} \tag{2}$$

where $\beta = 1/k_\mathrm{B}T$, k_B is Boltzmann's constant, and T is temperature. See Supporting Information section 2 for full ISDM results. Integration of the $R(z)$ profile allows calculation of an overall permeation coefficient P_eff

$$P_\mathrm{eff} = \frac{1}{R_\mathrm{eff}} = \frac{1}{\int_{-z_b}^{z_b} R(z)\,\mathrm{d}z} \tag{3}$$

where the integration extremes are in the water phase at either side of the membrane ($z_b = 40$ Å and $-z_b = -40$ Å). The membrane partitioning values of each drug molecule for the POPC membrane were determined from the PMF free energy curves using the standard binding free energy[72]

$$\Delta G_\mathrm{bind}^\circ = -k_\mathrm{B}T \ln\left(\frac{1}{z_b} \int_0^{z_b} \exp(-\beta \Delta G(z))\,\mathrm{d}z \right) \tag{4}$$

The membrane partitioning is then

$$K_\mathrm{lip} = \exp(-\beta \Delta G_\mathrm{bind}^\circ) \tag{5}$$

Final P_eff and K_lip values are the average of the independent runs ± standard deviation. The average number of hydrogen bonds each drug molecule makes to either lipid head groups or water molecules while partitioned was determined by counting hydrogen bonds using CPPTRAJ[73] using the trajectory of the PMF window corresponding to the energy minimum of the respective PMF profile for each compound. The hydrogen bond definition was a distance of 3.5 Å and an angle greater than 135°.

Kinetic Rate Constant Estimation with Markov State Models. The biased PMF results were combined with multiple short, unbiased MD simulations initiated at either the membrane center ($z = 0$ Å) or the water phase ($z = 40$ Å), in pyEMMA software.[74] The selection of these starting points along the z-axis reaction coordinate ensures the resulting

simulations are "downhill"; i.e., the drug molecule moves toward the equilibrium position just below the polar lipid head groups. For each of the seven drug molecules, 100 unbiased runs were performed starting from different initial conformations with the small molecule at $z = 0$ Å for 25 ns NPT, during which time the drug translocated to the equilibrium position just below the lipid head groups. A further 100 unbiased runs were performed per drug molecule initiated with different starting conformations in the water phase ($z = 40$ Å), with each simulation lasting 100 ns NPT; in almost all simulations, the drug partitioned into the membrane, positioning just below the lipid head groups.

We first derived the implied time scales in order to determine a suitable lag time by estimating Markov state models using the unbiased simulation data only at a series of lag times (1, 2, 3, 5, 7, and 10 timesteps of 10 ps); it was found that for all compounds a lag time of 1 time step was suitable as the ITSs are approximately flat with this lag time (see Supporting Information section 6). We then built a Markov state model using the unbiased simulation data and the stationary distribution from the previous PMF calculation with a lag time of 1 time step, allowing calculation of the kinetic quantities of the system.[48] It was found that there are three slow relaxation time scales; we therefore used the PCCA+ spectral clustering method to cluster the data into four metastable sets. In all cases, these four sets corresponded to the water phase on either side of the membrane and the equilibrium positions within the membrane just below the lipid head groups (see Supporting Information section 6).

The mean-first-passage times (MFPT) between these metastable sets therefore provides estimates of the rate constants k_in, k_out, and k_flip. Errors in kinetic rate constant values were determined as averages over the independent PMF runs ± standard deviation; the MSM procedure was performed using each of the independent PMF results with the unbiased simulation data for that compound, allowing kinetic rate constant estimates to be made for each independent free energy surface.

Comparison to Spontaneous Flip-Flop Runs. To investigate how well the PMF calculations capture the spontaneous flip-flop of small molecules across the membrane core, numerous unbiased simulations of propranolol, one of the molecules with higher experimental permeability, were run. A 72 POPC membrane with 30 waters per lipid and a single propranolol molecule partitioned just below the headgroup region was equilibrated for 50 ns at 303 K in the NPT ensemble. Then 250 independent simulations with different random velocities were performed, each for 100 ns each, amounting to a total of 25 μs of sampling. From these runs, three complete flip-flop events were observed; additionally, four half-events also occurred, whereby propranolol moved to the membrane center and then returned to the origin leaflet. These unbiased events allow investigation of the orientation and hydrogen bonding behavior during flip-flop and how well the biased PMF windows capture the true flip-flop event. It was found that for propranolol the molecular orientation and hydrogen bonding compare favorably between the unbiased flip-flop simulations and biased PMF windows (see Supporting Information section 5). Furthermore, WHAM may be applied to the unbiased simulation data to determine the free energy barrier to membrane flip-flop; this is found to be within the error bars of the umbrella sampling result (see Supporting Information section 5). These observations provide confidence

in the biased PMF results, at least for propranolol. However, the sampling required to perform the same comparison for the less permeable compounds limits extension to the full data set.

Dynamic Mechanistic Model of Passive Membrane Permeation. A kinetic model of liposome permeation was constructed in MATLAB,[75] following those outlined previously,[11,14−16] with parameters chosen such that it matches the experimental liposomal permeation assay setup.

It consists of movement between four compartments (see Figure 1) that is controlled by four coupled ordinary differential equations

$$\frac{dS_{AO}}{dt} = -k'_{in}S_{AO} + k'_{out}S_{LO}$$

$$\frac{dS_{LO}}{dt} = k'_{in}S_{AO} - (k'_{out} + k_{flip})S_{LO} + k_{flip}S_{LI}$$

$$\frac{dS_{LI}}{dt} = k''_{in}S_{AI} - (k''_{out} + k_{flip})S_{LI} + k_{flip}S_{LO}$$

$$\frac{dS_{AI}}{dt} = -k''_{in}S_{AI} + k''_{out}S_{LI} \qquad (6)$$

where S denotes the amount of substrate (drug molecule) in moles, AO is the outer aqueous phase, LO is the outer lipid layer, LI is the inner lipid layer, and AI is the inner aqueous phase. Note that the adsorption and desorption rate constants are dependent on surface area of the barrier and volume of the origin phase via $k = P\left(\frac{A}{V}\right)$, where P is the permeation coefficient, A denotes surface area, and V denotes volume. The observed rate constant estimates from MD simulations were converted to their respective P values using the surface area of the bilayer (POPC area per lipid 65.6 Å^2) and volumes of the water phase (TIP3P water volume 30.5 Å^3) and lipid phase (POPC volume per lipid 1205.4 Å^3).[58,76] The P values are therefore $P_{in}^{MD} = k_{in}^{MD}\left(\frac{V_{AO}^{MD}}{A_{LO}^{MD}}\right)$ and $P_{out}^{MD} = k_{out}^{MD}\left(\frac{V_{LO}^{MD}}{A_{LO}^{MD}}\right)$.

The rate constants for the mechanistic model were then determined using the appropriate surface areas and volumes of the liposome system as $k'_{in} = P_{in}^{MD}\left(\frac{A_{LO}}{V_{AO}}\right)$ and so forth.

The drug molecule amount was 10 μmol (entirely in the outer aqueous phase at time $t = 0$), and the liposome diameter was 200 nm in order to replicate experimental conditions.[22] The $V_{AO}:V_{LO}:V_{LI}:V_{AI}$ ratio of 1000:1:1:10, as identified by Thomae et al., was used to specify the volumes.[77]

The system was simulated until steady-state was achieved, and the resulting increase of substrate amount in the acceptor compartment (AI) was fitted to the biexponential function

$$S_{AI} = A\ e^{-k_a t} + B\ e^{-k_b t} \qquad (7)$$

where S_{AI} is the observed substrate amount in acceptor compartment AI, A and B are weighting coefficients, k_a and k_b are rate constants, and t is time. Permeation coefficients for movement across the entire membrane are then calculated using the rate constant k_a of the fastest phase via[22,78,79]

$$P = \frac{k_a r}{3} \qquad (8)$$

where r is the radius of the liposome (100 nm). This procedure to determine permeability coefficients from the compound

appearance in the acceptor compartment mirrors that used experimentally by Eyer et al.[22]

■ RESULTS

Free Energy and Kinetic Calculations. The free energy of transfer profiles (water → membrane) for the neutral form of each of the seven weak bases are plotted in Figure 3. All profiles
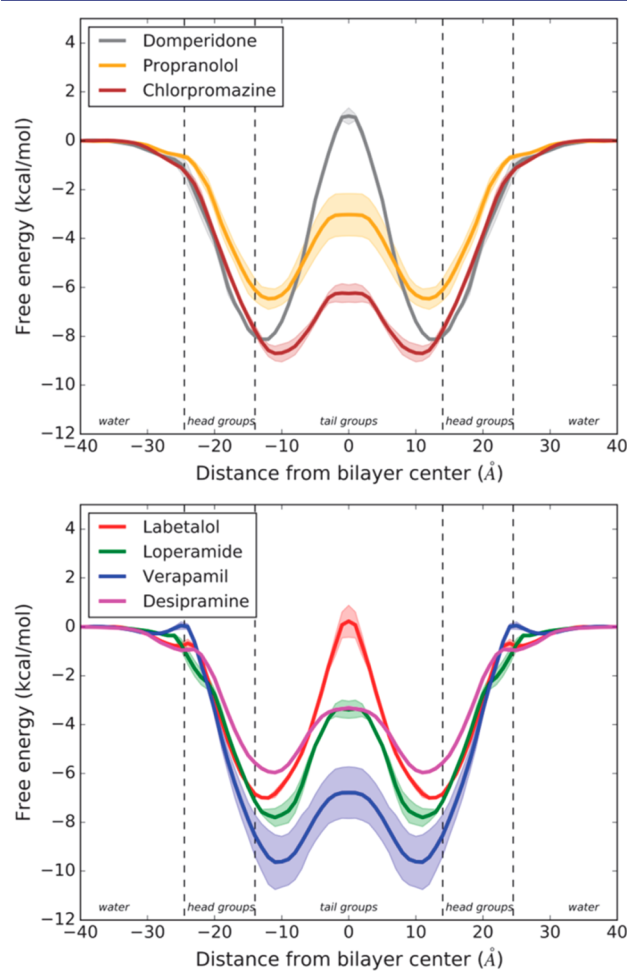

Figure 3. Free energy of transfer profiles (water → membrane) for the seven weakly basic small molecules under study. Results were calculated for one bilayer leaflet and assumed to be identical for the other leaflet by symmetry. The PMF is the average of two or more independent runs; the standard deviations are shown with shading.

have a similar shape: upon membrane entry, the free energy drops sharply to a minima just below the lipid head groups at approximately $z = 10$ Å from the bilayer center. Only verapamil shows a significant barrier to crossing the headgroup region of the membrane, possibly since this compound does not possess hydrogen bond donors and therefore cannot adequately replace water molecules solvating lipid head groups while crossing the membrane/water interface. Once inside the membrane at the free energy minimum, the barrier to move back into water is ΔG_{mem}. To instead transition across the membrane to the equivalent free energy minima at the opposite side, the compounds must undergo a flip-flop event across the hydrophobic membrane core, with barrier ΔG_{flip}. The two independent repeat PMFs for chlorpromazine, desipramine, domperidone, and loperamide yielded low error, reaching a maximum of ±0.35 kcal/mol or less at the membrane center.

Table 1. Permeability Coefficients from Experiment and Those Calculated Using the Inhomogeneous Solubility-Diffusion Model or the Dynamic Mechanistic Model with MD-Derived Kinetic Rate Constants

name	$\log(\mathrm{Perm_N}/[\mathrm{cm\ s^{-1}}])$ (experiment)	$\log(\mathrm{Perm_N}/[\mathrm{cm\ s^{-1}}])$ (ISDM)	k_{in} (s^{-1})	k_{out} (s^{-1})	k_{flip} (s^{-1})	$\log(\mathrm{Perm_N}/[\mathrm{cm\ s^{-1}}])$ (multiscale)
domperidone	−2.6	0.49 ± 0.09	1.48 ± 0.26 × 10⁹	1.76 ± 0.16 × 10³	3.50 ± 0.85 × 10²	−2.65 ± 0.11
labetalol	−2.1	0.90 ± 0.14	1.17 ± 0.06 × 10⁹	1.14 ± 0.18 × 10⁴	1.30 ± 0.88 × 10⁴	−1.20 ± 0.36
loperamide	−0.42	1.03 ± 0.03	8.59 ± 0.74 × 10⁸	1.81 ± 0.77 × 10³	6.71 ± 4.89 × 10⁵	0.11 ± 0.09
verapamil	0.01	0.89 ± 0.04	4.56 ± 0.61 × 10⁸	1.43 ± 1.23 × 10²	7.53 ± 4.09 × 10⁶	0.09 ± 0.05
propranolol	0.19	1.24 ± 0.04	1.27 ± 0.12 × 10⁹	3.09 ± 1.84 × 10⁴	4.75 ± 2.83 × 10⁶	0.51 ± 0.06
chlorpromazine	0.59	1.35 ± 0.01	1.94 ± 0.01 × 10⁹	7.75 ± 3.46 × 10²	1.74 ± 0.04 × 10⁷	0.85 ± 0.13
desipramine	0.65	1.26 ± 0.01	2.13 ± 0.93 × 10⁹	4.86 ± 1.27 × 10⁴	1.09 ± 0.02 × 10⁷	0.70 ± 0.10
			Correlation with Experimental Permeation			
r^2		0.76				0.94
mean absolute difference		1.55				0.31

However, the error for labetalol reaches ±0.66 kcal/mol at the membrane center; for propranolol, it rises to ±0.87 kcal/mol. Finally, verapamil required a third independent repeat PMF; even so, this compound yielded the maximum error at the membrane center of ±1.06 kcal/mol.

In order to obtain permeability coefficients from PMF calculations, typically the position-dependent diffusion values are determined for each window and combined via the ISDM to arrive at an overall permeation coefficient using eq 3. Values calculated with this method are given in Table 1 and plotted in Figure 4. The ISDM performs reasonably well in terms of rank ordering the compounds for permeation ($r^2 = 0.76$); however,

Figure 4. Correlation between experimental permeation coefficients and those calculated using (A) the inhomogeneous solubility-diffusion model and (B) multiscale model using MD-derived kinetic rate constants.

when comparing quantitatively with experiment, all permeation coefficients are overestimated (mean absolute difference = 1.55; gradient of trend line $m = 0.20$). These results are in-line with a previous study by Swift et al. which sought to validate the ISDM for permeation prediction, achieving $r^2 = 0.45$ between predicted and experimental values for 11 compounds; free energy profiles for propranolol and verapamil also compare favorably to those determined by Swift et al.[32] The numerical result of 17.4 cm s⁻¹ for propranolol is close to that of 10 and 14 cm s⁻¹ determined for the structurally very similar alprenalol using all-atom and mixed all-atom/coarse-grain simulations.[80,81]

We next turn to the results of the MD-derived kinetic rate constants and overall permeation estimate using the dynamic mechanistic model of permeation. On inspection of the values of the kinetic rate constants in Table 1, all k_{in} values are relatively similar ($\sim 1 \times 10^9$ s⁻¹), likely reflecting near diffusion-limited entry into the membrane, as observed experimentally by Eyer et al.[22] If k_{in} rate constants are roughly equivalent, then k_{out} values should depend solely on membrane partitioning of the compound, resulting in a range of k_{out} rate constants covering 2 orders of magnitude (1.43×10^2 to 4.86×10^4 s⁻¹). We find that flip-flop rate constants k_{flip} cover 5 orders of magnitude (3.50×10^2 to 1.74×10^7 s⁻¹); furthermore, they roughly rank compounds in order of experimental permeation. The kinetic rate constants of membrane entry k_{in} are comparable with experimental observations of k_{in} rate constant between 3.5×10^9 to 8.5×10^{10} s⁻¹ for aliphatic amine compounds.[82] Simulation results of k_{flip} have been reported for cholesterol (3×10^5 to 4.7×10^6 s⁻¹)[46] and oleic acid (0.22–0.28×10^6 s⁻¹)[44] that are comparable to k_{flip} values reported in Table 1.

Inserting each rate constant value into the dynamic mechanistic model of permeation then allows calculation of the time course of compound appearance in the acceptor compartment (i.e., the liposome inner aqueous layer in Figure 1), resulting in permeation profiles as shown in Figure 5. By fitting the resulting permeation profile to a biexponential function (eq 7), we can then estimate permeation coefficients by applying eq 8 (see Table 1). It is seen that these results give higher correlation with experiment than the ISDM, with $r^2 = 0.94$. Furthermore, the gradient of the trend line rises to $m = 0.94$ and the mean absolute difference with experiment decreases to 0.31.

Comparison of calculated membrane partitioning values with available experimental PC liposome partitioning data points reveals that the MD results for the most part overpredict membrane partitioning (see Table 2). This may be either due
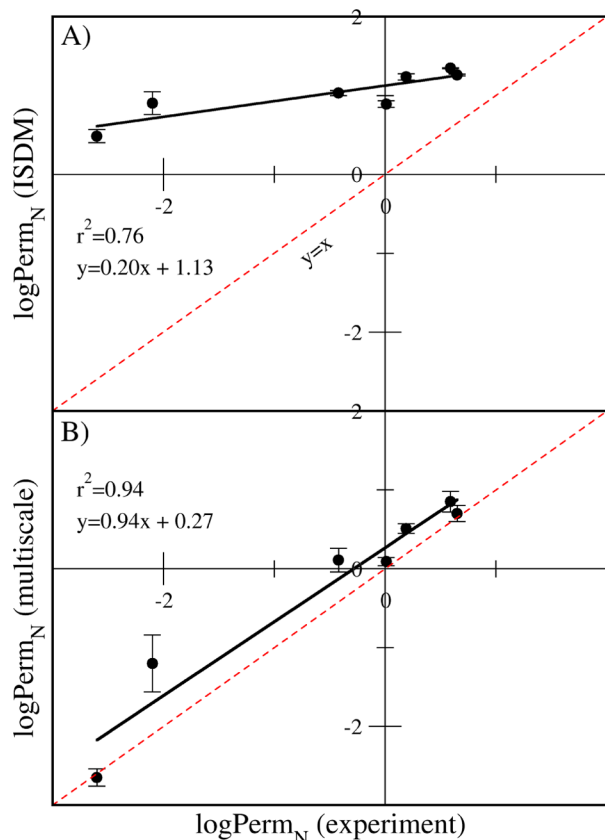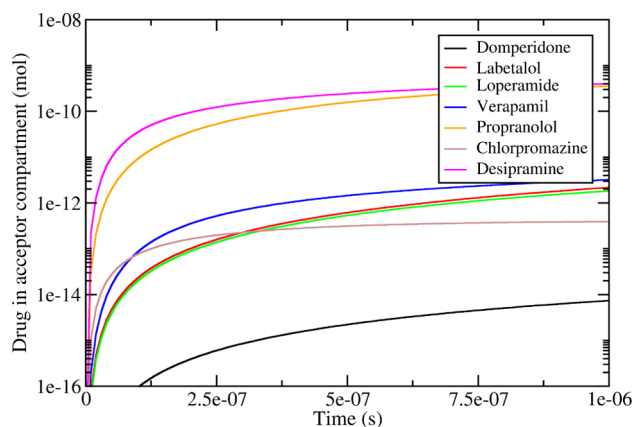
Figure 5. Change of drug amount in inner aqueous phase of liposome with time from simulations of the dynamic mechanistic model of permeation using MD-derived kinetic rate constants.

Table 2. Experimental Log P Values, Experimental PC Membrane Partitioning of Neutral Species, and Calculated PC Membrane Partitioning of Neutral Species from the PMF Results

name	log P	log $K_{\mathrm{lip},n}$	c log $K_{\mathrm{lip},n}$
domperidone	3.90		4.94 ± 0.004
labetalol	3.09		4.16 ± 0.04
loperamide	5.50		4.75 ± 0.22
verapamil	3.79	4.20[83]	6.07 ± 0.76
propranolol	3.48	3.35[84]	3.81 ± 0.31
chlorpromazine	5.41	4.45[84]	5.44 ± 0.22
desipramine	4.90	4.05[85]	3.47 ± 0.01

to the choice of force field, the charge derivation method, or rather a limitation of fixed charge force fields; previous work has found improved prediction of membrane partitioning by including polarizability.[72] A further discrepancy may be the difference in lipid composition: experiments used liposomes of egg PC or PhC, whereas simulations used pure POPC bilayers.

Structure−Kinetic Relationships of Membrane Permeation. On analysis of Table 1, it is seen that either the k_{flip} rate constant or the k_{out} rate constant may be the slowest process in overall membrane translocation. Of the seven compounds, only domperidone has a k_{flip} rate constant lower than k_{out}, meaning that for this compound the flip-flop process is the slowest step. On comparison of the domperidone chemical structure (Figure 2) with the second slowest permeating compound, labetalol, it may be surprising that domperidone has a lower flip-flop than labetalol: domperidone has log P 3.9, a hydrogen bond donor (HBD) count of 2, and a hydrogen bond acceptor (HBA) count of 7; conversely, labetalol has a lower log P of 3.09, HBD 5, and HBA 5. We would likely expect labetalol to have slower movement across the hydrophobic membrane core due to its lower log P and greater number of HBDs. However, the structure of labetalol is essentially "lipid-like" given that is has a hydrophobic tail and hydrophilic headgroup region, meaning that when partitioned in the membrane it orientates along the membrane normal. Domperidone has no such separation of hydrophobic and hydrophilic regions, and when partitioned, it orientates along the membrane/water interface (see Supporting Information section 4), leaving it more solvent exposed. Labetalol has the additional advantage of being able to form up to two

intramolecular hydrogen bonds, shielding HBDs when located in the low dielectric medium of the membrane, an ability that has been linked to enhanced membrane permeation.[86,87] The flip-flop process, rather than being determined by compound hydrophobicity, is likely limited by desolvation cost to leave the membrane partitioned position.[35] Indeed, we find that this combination of intramembrane orientation and internal hydrogen bonding (see Figure 6) translates to lower solvation
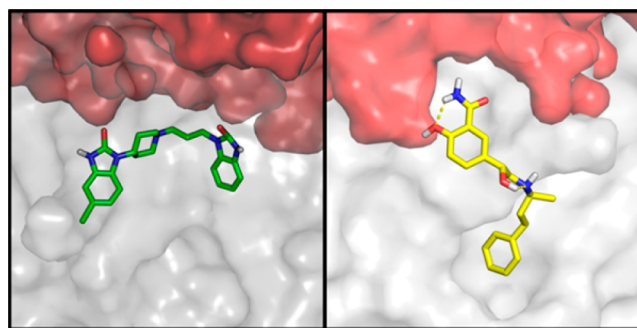

Figure 6. Intramembrane orientation of domperidone (left) and labetalol (right) while at the energy minima position within the membrane and below lipid head groups. Labetalol is able to form two intramolecular hydrogen bonds (dashed yellow lines). Membrane lipids are shown in a gray surface; water is shown as a red surface.

of labetalol while partitioned in the membrane compared to domperideone; by counting the average number of hydrogen bonds formed between the molecules and either water or lipid head groups when partitioned in the membrane, we find that domperidone forms on average 4.4 H-bonds, whereas labetalol makes 4.23. The slower flip-flop of domperidone due to its higher membrane partitioned solvation, combined with lower k_{out}, translates into making it the slowest permeating compound of the set.

Although the flip-flop rate constant may be rate-limiting for certain molecules, in other instances the k_{out} rate constant may limit permeation. Comparison of propranolol and verapamil reveals that although propranolol has a lower k_{flip} than verapamil, it has a much higher k_{out} due to lower membrane partitioning and faster overall permeation. In this case, the molecular descriptors of verapamil and propranolol align with their respective flip-flop rate constants: verapamil has log P 3.79, HBD 0, and HBA 6, whereas propranolol has log P 3.48, HBD 2, and HBA 3. The more hydrophilic propranolol therefore has the lower flip-flop rate constant. Furthermore, their solvation while partitioned lines up with flip-flop cost as verapamil has fewer H-bonds while partitioned (0.78) versus propranolol (1.69).

Both desipramine and chlorpromazine have similar k_{flip} values (1.09 × 10^7 to 1.74 × 10^7 s⁻¹) and structurally are also very similar. As with the previous example, we find that in this case k_{out} is the rate-limiting step, with the k_{out} value of chlorpromazine being lower than that of desipramine. This arises due to the differing membrane partitioning of the two compounds: desipramine has a log P of 4.9, whereas chlorpromazine has a log P of 5.41, which translates into experimental log $K_{\mathrm{lip},n}$ values of 4.05 and 4.45, respectively. This may be due to the presence of one HBD on desipramine, whereas chlorpromazine has no HBDs.

A final point of interest is the most hydrophobic molecule in the data set. Loperamide has the highest log P value of 5.5, yet

it has intermediate membrane permeation (log Perm_N = -0.42). Despite being the most lipophilic, loperamide has one of the lowest k_{flip} values, being higher than only domperidone and labetalol. Once again, we find that the flip-flop rate constant is better predicted from the desolvation cost to leave the equilibrium partitioned position just below the lipid head groups; loperamide forms an average number of 2.0 hydrogen bonds with either water or lipid while partitioned in the membrane, correctly ranking the barrier to flip-flop as lower than domperidone or labetalol yet higher than the remainder of the set (see Supporting Information section 3 for full list of H-bonds while partitioned values). An interesting comparison point is with propranolol due to their similar molecular properties: loperamide has HBD 1 and HBA 4, whereas propranolol has HBD 2 and HBA 3. We could therefore expect propranolol to form more hydrogen bonds with water or lipid while partitioned due to higher HBD and therefore have a lower rate of flip-flop than loperamide. However, as with labetalol, the structure of propranolol is more "lipid-like", resulting in a membrane partitioned orientation along the membrane normal, whereas loperamide orientates along the membrane/water interface (see Supporting Information section 4). Furthermore, propranolol has the ability to shield one HBD by forming an intramolecular hydrogen bond. These features result in fewer H-bonds while partitioned and a lower desolvation cost to flip-flop for propranolol, meaning a lower barrier to move across the membrane core and higher k_{flip} rate constant.

From the structure–kinetics relationships investigated, we find that either k_{flip} or k_{out} may be the slowest step to membrane permeation, with the combination of the two rate constants deciding overall translocation rate. The k_{out} is determined by membrane partitioning, which generally follows log P.[88] The k_{flip} rate constant is best predicted from hydrogen bonding of the compound to water or lipid while partitioned in the membrane. The number of hydrogen bonds while partitioned does not necessarily follow the sum of HBD and HBA as could be expected (see Supporting Information section 3): intramembrane orientation and ability to shield HBDs also play an important role.

Finally, we note that, for this data set, overall membrane permeation trends with the rank order of k_{flip} rate constants. The rate constant of flip-flop k_{flip} is determined by the free energy barrier ΔG_{flip}, which in turn depends primarily on loss of hydrogen bonds to leave the membrane partitioned position (see ΔG_{flip} and H-bond count correlation in Supporting Information section 3). We therefore find a strong correlation between overall experimental permeation and the average number of hydrogen bonds each compound makes with either lipid or water while partitioned at equilibrium position in the membrane (see Figure 7). Consequently, this value, which may be calculated from a single MD run, may potentially serve as a suitable virtual predictor for membrane permeation, in particular when k_{out} is not a deciding factor.

■ DISCUSSION

In this work, we study membrane permeation for a set of well-characterized compounds using all-atom simulations and a dynamic mechanistic model, finding good quantitative agreement with experiment when combining kinetic rate constants derived from MD into the dynamic model of in vitro liposome permeation. This level of agreement with experiment cannot be matched with the ISDM as applied to PMF calculations.
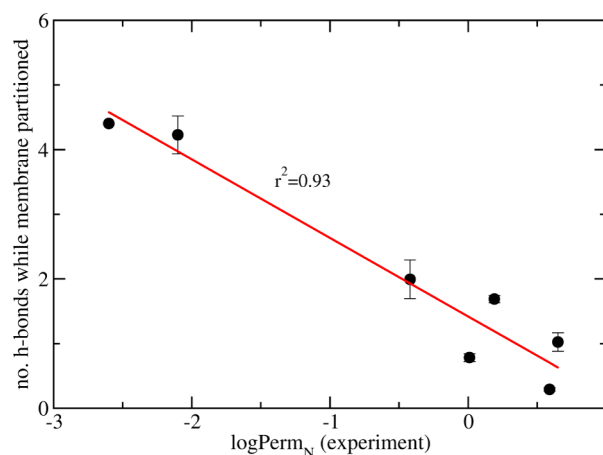

Figure 7. Correlation between average number of hydrogen bonds formed with lipid or water while membrane partitioned and experimental permeation.

Furthermore, the calculation of kinetic rate constants allows us to build structure–kinetic relationships of permeation and investigate each step in the overall process. Such structure–kinetic relationships may aid in optimization of chemical structures for membrane permeation and related ADME-Tox properties. As predicted from the kinetic model of permeation (Figure 1), we find that overall permeation depends on two counterbalanced processes: k_{out} (maximized by decreasing membrane partitioning) and k_{flip} (maximized by lowering the number of hydrogen bonds that must be lost to allow flip-flop). Optimal permeation therefore depends on balancing membrane partitioning with enthalpy cost to flip-flop; membrane partitioning should not be lowered to the extent that k_{in} becomes rate-limiting. Obtaining rate constants allows us to investigate the effect of differences in given energy barriers encountered during membrane translocation on the overall rate of membrane permeation.

In essence, both the ISDM and the dynamic mechanistic model take as input the same information: the free energy landscape calculated for the movement of each molecule across the membrane. The ISDM then uses position-dependent diffusion values from which the local resistances are determined; finally, these are integrated to yield an overall resistance to permeation, the inverse of the permeability coefficient. The local resistances depend exponentially on the free energy yet only linearly on the local diffusion; the position-dependent resistances therefore closely follow the free energy profile. On the other hand, the dynamic mechanistic model takes only three rate constants, which are proportional to the ΔG_{flip} and ΔG_{mem} barriers encountered on the free energy landscape. It therefore appears that the better agreement with experiment of the dynamic model is not due to the atomistic computation but how this data is treated by the theoretical model of permeation. Whereas the ISDM assumes that permeation is limited by diffusion through a single membrane barrier, the dynamic model breaks the permeation process down into each step, with overall permeation being determined by the kinetic rate constants linking each stage in the event. Furthermore, the dynamic model allows incorporation of concentration differences at each position and the surface area to volume ratios.

In the dynamic mechanistic model of permeation, movement between each position depends not only on the kinetic rate

constants linking compartments but also the concentration of small molecule in each compartment. The compound first partitions into the membrane with rate constant k_{in}; the concentration of small molecule partitioned in the membrane at the lipid outer position depends on the membrane partitioning K_{lip} as controlled by k_{out}. The next step, flip-flop across the hydrophobic core, therefore depends both on the k_{flip} rate constant and also the concentration of drug at the lipid outer position. Higher membrane partitioning may compensate for a lower k_{flip} rate constant. After flip-flop, the compound must exit the membrane with rate constant k_{out}; however, again this depends on the concentration of drug able to reach the lipid inner position. With higher k_{flip}, there is greater concentration at the lipid inner layer which may swamp the k_{out} step; with lower k_{flip}, there is reduced concentration available to leave the membrane. This is likely why, for this data set, overall membrane permeation depends strongly on k_{flip} rate constant: compounds with higher k_{flip} allow greater concentrations to reach the lipid inner region and the k_{out} may proceed quickly. However, with lower k_{flip}, reduced concentration is present to desorb from the membrane, which limits overall membrane translocation. Using the ISDM, permeation of a single molecule depends on each free energy barrier and there is no dependence on molecular concentration available at each position; this may explain the poorer performance of the ISDM for lipophilic drug-like compounds.

For this data set, the overall membrane permeation depends strongly on the k_{flip} rate constant, which dictates both the ability of compound to flip-flop and also the concentration of drug able to reach the lipid inner layer, influencing the desorption into the liposome interior. The free energy barrier to flip-flop therefore correlates extremely well with experimental permeation, which may simply be estimated from the average number of hydrogen bonds each molecule makes with lipid or water while it is membrane partitioned. Furthermore, the atomistic detail afforded by MD simulations allows us to probe the structural features that minimize hydrogen bonds to water and lipid while partitioned; we find that in addition to the number of HBDs and HBAs, intramembrane orientation and intramolecular hydrogen bonding are important. The permeation profiles obtained from the dynamic mechanistic model of permeation qualitatively match those from experimental liposomal permeation studies,[22] as could be expected when using a kinetic model of permeation which best represents the in vitro process. Furthermore, the advantage of such a model is that it may be extended to better represent either a more complicated in vitro system or potentially in vivo permeation, with the caveat that we require all rates and concentrations involved for such an extension.

Permeation profiles and coefficients were determined for the neutral form of seven basic small molecules; these values can then be converted to those for the charged population of the compound at pH 7.4 via the Henderson−Hasselbalch relationship, which is the inverse of the procedure used by Eyer et al. to determine the permeability of the neutral species. However, it should be noted that even a small shift in the pK_a value used for this calculation can have substantial effects. Furthermore, all-atom simulations used entirely the neutral form of the compound given that permeation of the cationic form through the membrane is expected to be minimal.[23] It is possible that the cationic form of the molecule first partitions into the membrane, becoming neutral only prior to flip-flop, given the known attraction between cationic drug molecules and lipid

membranes.[89] Although this may speed k_{in} values, these were never rate-limiting in overall permeation.

The calculation of kinetic processes using MD simulation with fixed charged force fields is a relatively new area;[90,91] simulation and analysis protocols are therefore still being established. To date, few studies have examined force field dependence of kinetic processes.[92] Furthermore, the underlying free energy surface may not accurately represent the system, which may also impact on kinetic calculations; in this work, we find that for certain molecules the calculated membrane partitioning does not match experiment. The effect of force fields and inclusion of polarization on membrane partitioning has received attention previously[72,93] and would be an interesting follow-up study for the current data set. Additionally, the current work assumed only the small molecule movement along the membrane normal to be the reaction coordinate of significance; however, a number of studies have investigated the effect of other orthogonal slowly relaxing degrees of freedom, such as small molecule orientation and lipid headgroup reorganization.[94−98] This work could, in the future, be extended beyond a 1D reaction coordinate with the correct selection of collective variables. Regardless, the combination of MD-derived kinetic rate constants into a wider systems-level model is an exciting development of in silico all-atom simulation and may, in the future, allow the detailed investigation of drug permeation and protein binding in the wider context of a cellular system.

In order to extend our study to capture passive permeation through realistic cell membranes, we must account for the variable lipid composition and, furthermore, the asymmetric distribution of lipid species and ions between the extracellular and intracellular membrane layers. In this work, we used POPC given that the experimental values were obtained using liposomes composed of this lipid species; however, the ability to model membranes of mixed lipid composition using molecular dynamics and associated force fields[58,99−105] may allow future work to expand the present model to include a more comprehensive representation of the cell membrane, particularly given that membrane lipid composition has been found to alter liposomal permeation.[77]

CONCLUSIONS

Combining all-atom MD simulations and a dynamic mechanistic model of membrane permeation allows a detailed investigation of each step involved in the membrane translocation event and derivation of structure−kinetics relationships of passive membrane permeation. We find that either k_{flip} or k_{out} may be the slowest step in overall permeation; however, for the data set under study, the k_{flip} rate constants essentially dictate permeation. In order to optimize this rate, we must lower hydrogen bonding to water or lipid while partitioned in the membrane; this depends on intramembrane orientation, HBD and HBA count, and the ability to shield HBDs. Finally, the number of hydrogen bonds while partitioned metric may efficiently rank compounds by overall permeation rate and could potentially serve as a valuable virtual screening descriptor.

ASSOCIATED CONTENT

ⓢ Supporting Information

The Supporting Information is available free of charge on the ACS Publications website at DOI: 10.1021/jacs.6b11215.

Convergence of PMF profiles, full ISDM outputs, depth-dependent hydrogen bonding and molecular orientation details, spontaneous flip-flop comparison, Markov state model outputs, results of biexponential fits, and compound topologies (PDF)

■ AUTHOR INFORMATION

Corresponding Author
*callum.dickson@novartis.com

ORCID ⬤
Callum J. Dickson: 0000-0003-4013-6394

Notes
The authors declare no competing financial interest.

■ REFERENCES

(1) Smith, D.; Artursson, P.; Avdeef, A.; Di, L.; Ecker, G. F.; Faller, B.; Houston, J. B.; Kansy, M.; Kerns, E. H.; Krämer, S. D.; Lennernäs, H.; van de Waterbeemd, H.; Sugano, K.; Testa, B. *Mol. Pharmaceutics* **2014**, *11*, 1727.
(2) Avdeef, A. *Absorption and Drug Development: Solubility, Permeability, and Charge State*; Wiley: Hoboken, NJ, 2003.
(3) Di, L.; Whitney-Pickett, C.; Umland, J. P.; Zhang, H.; Zhang, X.; Gebhard, D. F.; Lai, Y.; Federico, J. J.; Davidson, R. E.; Smith, R.; Reyner, E. L.; Lee, C.; Feng, B.; Rotter, C.; Varma, M. V.; Kempshall, S.; Fenner, K.; El-kattan, A. F.; Liston, T. E.; Troutman, M. D. *J. Pharm. Sci.* **2011**, *100*, 4974.
(4) Hurst, D. P.; Schmeisser, M.; Reggio, P. H. *Chem. Phys. Lipids* **2013**, *169*, 46.
(5) Zhang, D.; Gao, Z.-G.; Zhang, K.; Kiselev, E.; Crane, S.; Wang, J.; Paoletta, S.; Yi, C.; Ma, L.; Zhang, W.; Han, G. W.; Liu, H.; Cherezov, V.; Katritch, V.; Jiang, H.; Stevens, R. C.; Jacobson, K. A.; Zhao, Q.; Wu, B. *Nature* **2015**, *520*, 317.
(6) Overton, E. *Studien über die Narkose. Zugleich ein Beitrag zur allgemeinen Pharmakologie*; Gustav Fischer: Jena, Germany, 1901.
(7) Finkelstein, A. *J. Gen. Physiol.* **1976**, *68*, 127.
(8) Nagle, J. F.; Tristram-Nagle, S. *Biochim. Biophys. Acta, Rev. Biomembr.* **2000**, *1469*, 159.
(9) Diamond, J.; Katz, Y. *J. Membr. Biol.* **1974**, *17*, 121.
(10) Marrink, S. J.; Berendsen, H. J. C. *J. Phys. Chem.* **1994**, *98*, 4155.
(11) Krämer, S. D.; Lombardi, D.; Primorac, A.; Thomae, A. V.; Wunderli-Allenspach, H. *Chem. Biodiversity* **2009**, *6*, 1900.
(12) Ghaemi, Z.; Alberga, D.; Carloni, P.; Laio, A.; Lattanzi, G. *J. Chem. Theory Comput.* **2016**, *12*, 4093.
(13) Kamp, F.; Hamilton, J. A. *Prostaglandins, Leukotrienes Essent. Fatty Acids* **2006**, *75*, 149.
(14) Filipe, H. A. L.; Salvador, A.; Silvestre, J. M.; Vaz, W. L. C.; Moreno, M. J. *Mol. Pharmaceutics* **2014**, *11*, 3696.
(15) Penniston, J. T.; Beckett, L.; Bentley, D. L.; Hansch, C. *Mol. Pharmacol.* **1969**, *5*, 333.
(16) Grassi, M.; Coceani, N.; Magarotto, L. *Int. J. Pharm.* **2002**, *239*, 157.
(17) Läuger, P.; Benz, R.; Stark, G.; Bamberg, E.; Jordan, P. C.; Fahr, A.; Brock, W. *Q. Rev. Biophys.* **1981**, *14*, 513.
(18) Nagle, J. F.; Mathai, J. C.; Zeidel, M. L.; Tristram-Nagle, S. *J. Gen. Physiol.* **2008**, *131*, 77.
(19) Oruc, T.; Kucuk, S. E.; Sezer, D. *Phys. Chem. Chem. Phys.* **2016**, *18*, 24511.
(20) Paloncýová, M.; DeVane, R.; Murch, B.; Berka, K.; Otyepka, M. *J. Phys. Chem. B* **2014**, *118*, 1030.
(21) Liu, X.; Testa, B.; Fahr, A. *Pharm. Res.* **2011**, *28*, 962.
(22) Eyer, K.; Paech, F.; Schuler, F.; Kuhn, P.; Kissner, R.; Belli, S.; Dittrich, P. S.; Krämer, S. D. *J. Controlled Release* **2014**, *173*, 102.
(23) Avdeef, A.; Box, K. J.; Comer, J. E. A.; Hibbert, C.; Tam, K. Y. *Pharm. Res.* **1998**, *15*, 209.
(24) Xiang, T.-X.; Anderson, B. D. *Adv. Drug Delivery Rev.* **2006**, *58*, 1357.
(25) Wilson, M. A.; Pohorille, A. *J. Am. Chem. Soc.* **1996**, *118*, 6580.
(26) Ulander, J.; Haymet, A. D. J. *Biophys. J.* **2003**, *85*, 3475.
(27) Bemporad, D.; Essex, J. W.; Luttmann, C. *J. Phys. Chem. B* **2004**, *108*, 4875.
(28) Orsi, M.; Sanderson, W. E.; Essex, J. W. *J. Phys. Chem. B* **2009**, *113*, 12019.
(29) MacCallum, J. L.; Bennett, W. F. D.; Tieleman, D. P. *J. Gen. Physiol.* **2007**, *129*, 371.
(30) Tejwani, R. W.; Davis, M. E.; Anderson, B. D.; Stouch, T. R. *J. Pharm. Sci.* **2011**, *100*, 2136.
(31) Paloncýová, M.; Berka, K.; Otyepka, M. *J. Chem. Theory Comput.* **2012**, *8*, 1200.
(32) Swift, R. V.; Amaro, R. E. *Chem. Biol. Drug Des.* **2013**, *81*, 61.
(33) Carpenter, T. S.; Kirshner, D. A.; Lau, E. Y.; Wong, S. E.; Nilmeier, J. P.; Lightstone, F. C. *Biophys. J.* **2014**, *107*, 630.
(34) Comer, J.; Schulten, K.; Chipot, C. *J. Chem. Theory Comput.* **2014**, *10*, 554.
(35) Marrink, S. J.; Berendsen, H. J. C. *J. Phys. Chem.* **1996**, *100*, 16729.
(36) Cardenas, A. E.; Elber, R. *J. Chem. Phys.* **2014**, *141*, 054101.
(37) Cardenas, A. E.; Jas, G. S.; DeLeon, K. Y.; Hegefeld, W. A.; Kuczera, K.; Elber, R. *J. Phys. Chem. B* **2012**, *116*, 2739.
(38) Cardenas, A. E.; Elber, R. *Mol. Phys.* **2013**, *111*, 3565.
(39) Votapka, L. W.; Lee, C. T.; Amaro, R. E. *J. Phys. Chem. B* **2016**, *120*, 8606.
(40) Bochicchio, D.; Panizon, E.; Ferrando, R.; Monticelli, L.; Rossi, G. *J. Chem. Phys.* **2015**, *143*, 144108.
(41) Ghaemi, Z.; Minozzi, M.; Carloni, P.; Laio, A. *J. Phys. Chem. B* **2012**, *116*, 8714.
(42) Sun, R.; Dama, J. F.; Tan, J. S.; Rose, J. P.; Voth, G. A. *J. Chem. Theory Comput.* **2016**, *12*, 5157.
(43) Tian, J.; Sethi, A.; Swanson, B. I.; Goldstein, B.; Gnanakaran, S. *Biophys. J.* **2013**, *104*, 622.
(44) Wei, C.; Pohorille, A. *J. Phys. Chem. B* **2014**, *118*, 12919.
(45) Choubey, A.; Kalia, R. K.; Malmstadt, N.; Nakano, A.; Vashishta, P. *Biophys. J.* **2013**, *104*, 2429.
(46) Bennett, W. F. D.; MacCallum, J. L.; Hinner, M. J.; Marrink, S. J.; Tieleman, D. P. *J. Am. Chem. Soc.* **2009**, *131*, 12714.
(47) Bennett, W. F. D.; Tieleman, D. P. *J. Lipid Res.* **2012**, *53*, 421.
(48) Prinz, J.-H.; Wu, H.; Sarich, M.; Keller, B.; Senne, M.; Held, M.; Chodera, J. D.; Schütte, C.; Noé, F. *J. Chem. Phys.* **2011**, *134*, 174105.
(49) Wishart, D. S.; Knox, C.; Guo, A. C.; Shrivastava, S.; Hassanali, M.; Stothard, P.; Chang, Z.; Woolsey, J. *Nucleic Acids Res.* **2006**, *34*, D668.
(50) Bayly, C. I.; McKay, D.; Truchon, J.-F. An Informal AMBER Small Molecule Force Field: parm@Frosst. http://www.ccl.net/cca/data/parm_at_Frosst/ (accessed April 22, 2016).
(51) Hornak, V.; Abel, R.; Okur, A.; Strockbine, B.; Roitberg, A.; Simmerling, C. *Proteins: Struct., Funct., Genet.* **2006**, *65*, 712.
(52) Jakalian, A.; Bush, B. L.; Jack, D. B.; Bayly, C. I. *J. Comput. Chem.* **2000**, *21*, 132.
(53) Jakalian, A.; Jack, D. B.; Bayly, C. I. *J. Comput. Chem.* **2002**, *23*, 1623.
(54) Beauchamp, K. A.; Behr, J. M.; Rustenburg, A. S.; Bayly, C. I.; Kroenlein, K.; Chodera, J. D. *J. Phys. Chem. B* **2015**, *119*, 12912.
(55) Velez-Vega, C.; McKay, D. J. J.; Aravamuthan, V.; Pearlstein, R.; Duca, J. S. *J. Chem. Inf. Model.* **2014**, *54*, 3344.
(56) Dickson, C. J.; Rosso, L.; Betz, R. M.; Walker, R. C.; Gould, I. R. *Soft Matter* **2012**, *8*, 9617.

(57) Skjevik, Å. A.; Madej, B. D.; Walker, R. C.; Teigen, K. *J. Phys. Chem. B* **2012**, *116*, 11124.

(58) Dickson, C. J.; Madej, B. D.; Skjevik, Å. A.; Betz, R. M.; Teigen, K.; Gould, I. R.; Walker, R. C. *J. Chem. Theory Comput.* **2014**, *10*, 865.

(59) Jorgensen, W. L.; Chandrasekhar, J.; Madura, J. D.; Impey, R. W.; Klein, M. L. *J. Chem. Phys.* **1983**, *79*, 926.

(60) Case, D. A.; Betz, R. M.; Botello-Smith, W.; Cerutti, D. S.; Cheatham, T. E.; Darden, T. A.; Duke, R. E.; Giese, T. J.; Gohlke, H.; Goetz, A. W.; Homeyer, N.; Izadi, S.; Janowski, P.; Kaus, J.; Kovalenko, A.; Lee, T. S.; LeGrand, S.; Li, P.; Lin, C.; Luchko, T.; Luo, R.; Madej, B.; Mermelstein, D.; Merz, K. M.; Monard, G.; Nguyen, H.; Nguyen, H. T.; Omelyan, I.; Onufriev, A.; Roe, D. R.; Roitberg, A.; Sagui, C.; Simmerling, C. L.; Swails, J.; Walker, R. C.; Wang, J.; Wolf, R. M.; Wu, X.; Xiao, L.; York, D. M.; Kollman, P. A. *AMBER 2016*; University of California: San Francisco, 2016.

(61) Götz, A. W.; Williamson, M. J.; Xu, D.; Poole, D.; Le Grand, S.; Walker, R. C. *J. Chem. Theory Comput.* **2012**, *8*, 1542.

(62) Salomon-Ferrer, R.; Götz, A. W.; Poole, D.; Le Grand, S.; Walker, R. C. *J. Chem. Theory Comput.* **2013**, *9*, 3878.

(63) Le Grand, S.; Götz, A. W.; Walker, R. C. *Comput. Phys. Commun.* **2013**, *184*, 374.

(64) Press, W. H.; Teukolsky, S. A.; Vetterling, W. T.; Flannery, B. P. *Numerical Recipes: The Art of Scientific Computing*; 3rd ed.; Cambridge University Press: New York, 2007; p 515.

(65) Pastor, R.; Brooks, B.; Szabo, A. *Mol. Phys.* **1988**, *65*, 1409.

(66) Berendsen, H. J. C.; Postma, J. P. M.; van Gunsteren, W. F.; DiNola, A.; Haak, J. R. *J. Chem. Phys.* **1984**, *81*, 3684.

(67) Ryckaert, J.-P.; Ciccotti, G.; Berendsen, H. J. C. *J. Comput. Phys.* **1977**, *23*, 327.

(68) Darden, T.; York, D.; Pedersen, L. *J. Chem. Phys.* **1993**, *98*, 10089.

(69) Filipe, H. A. L.; Moreno, M. J.; Róg, T.; Vattulainen, I.; Loura, L. M. S. *J. Phys. Chem. B* **2014**, *118*, 3572.

(70) Grossfield, A. *WHAM: the weighted histogram analysis method*, 2.0.9 ed.; University of Rochester, 2013.

(71) Hummer, G. *New J. Phys.* **2005**, *7*, 34.

(72) Jambeck, J. P. M.; Lyubartsev, A. P. *Phys. Chem. Chem. Phys.* **2013**, *15*, 4677.

(73) Roe, D. R.; Cheatham, T. E. *J. Chem. Theory Comput.* **2013**, *9*, 3084.

(74) Scherer, M. K.; Trendelkamp-Schroer, B.; Paul, F.; Pérez-Hernández, G.; Hoffmann, M.; Plattner, N.; Wehmeyer, C.; Prinz, J.-H.; Noé, F. *J. Chem. Theory Comput.* **2015**, *11*, 5525.

(75) *MATLAB*, R2015b ed.; Mathworks: Natick, MA, 2015.

(76) Rosso, L.; Gould, I. R. *J. Comput. Chem.* **2008**, *29*, 24.

(77) Thomae, A.; Koch, T.; Panse, C.; Wunderli-Allenspach, H.; Krämer, S. *Pharm. Res.* **2007**, *24*, 1457.

(78) Verkman, A. S.; Dix, J. A.; Seifter, J. L. *Am. J. Physiol.* **1985**, *248*, F650.

(79) Paula, S.; Volkov, A. G.; Deamer, D. W. *Biophys. J.* **1998**, *74*, 319.

(80) Bemporad, D. Ph.D. Thesis, University of Southampton, Southampton, United Kingdom, 2003.

(81) Orsi, M. Ph.D. Thesis, University of Southampton, Southampton, United Kingdom, 2008.

(82) Cardoso, R. M. S.; Martins, P. A. T.; Gomes, F.; Doktorovova, S.; Vaz, W. L. C.; Moreno, M. J. *J. Phys. Chem. B* **2011**, *115*, 10098.

(83) Meier, M.; Blatter, X. L.; Seelig, A.; Seelig, J. *Biophys. J.* **2006**, *91*, 2943.

(84) Pallicer, J. M.; Krämer, S. D. *J. Pharm. Biomed. Anal.* **2012**, *71*, 219.

(85) Marenchino, M.; Alpstäg-Wöhrle, A. L.; Christen, B.; Wunderli-Allenspach, H.; Krämer, S. D. *Eur. J. Pharm. Sci.* **2004**, *21*, 313.

(86) Rezai, T.; Yu, B.; Millhauser, G. L.; Jacobson, M. P.; Lokey, R. S. *J. Am. Chem. Soc.* **2006**, *128*, 2510.

(87) Alex, A.; Millan, D. S.; Perez, M.; Wakenhut, F.; Whitlock, G. A. *MedChemComm* **2011**, *2*, 669.

(88) Endo, S.; Escher, B. I.; Goss, K.-U. *Environ. Sci. Technol.* **2011**, *45*, 5912.

(89) Abdiche, Y. N.; Myszka, D. G. *Anal. Biochem.* **2004**, *328*, 233.

(90) Pande, V. S.; Beauchamp, K.; Bowman, G. R. *Methods* **2010**, *52*, 99.

(91) Chodera, J. D.; Noé, F. *Curr. Opin. Struct. Biol.* **2014**, *25*, 135.

(92) Vitalini, F.; Mey, A. S. J. S.; Noé, F.; Keller, B. G. *J. Chem. Phys.* **2015**, *142*, 084101.

(93) Paloncýová, M.; Fabre, G.; DeVane, R. H.; Trouillas, P.; Berka, K.; Otyepka, M. *J. Chem. Theory Comput.* **2014**, *10*, 4143.

(94) Neale, C.; Bennett, W. F. D.; Tieleman, D. P.; Pomès, R. *J. Chem. Theory Comput.* **2011**, *7*, 4175.

(95) Neale, C.; Madill, C.; Rauscher, S.; Pomès, R. *J. Chem. Theory Comput.* **2013**, *9*, 3686.

(96) Jämbeck, J. P. M.; Lyubartsev, A. P. *J. Phys. Chem. Lett.* **2013**, *4*, 1781.

(97) Parisio, G.; Stocchero, M.; Ferrarini, A. *J. Chem. Theory Comput.* **2013**, *9*, 5236.

(98) Comer, J.; Schulten, K.; Chipot, C. *J. Chem. Theory Comput.* **2014**, *10*, 2710.

(99) Madej, B. D.; Gould, I. R.; Walker, R. C. *J. Phys. Chem. B* **2015**, *119*, 12424.

(100) Jämbeck, J. P. M.; Lyubartsev, A. P. *J. Phys. Chem. B* **2012**, *116*, 3164.

(101) Jämbeck, J. P. M.; Lyubartsev, A. P. *J. Chem. Theory Comput.* **2012**, *8*, 2938.

(102) Jämbeck, J. P. M.; Lyubartsev, A. P. *J. Chem. Theory Comput.* **2013**, *9*, 774.

(103) Klauda, J. B.; Venable, R. M.; Freites, J. A.; O'Connor, J. W.; Tobias, D. J.; Mondragon-Ramirez, C.; Vorobyov, I.; MacKerell, A. D.; Pastor, R. W. *J. Phys. Chem. B* **2010**, *114*, 7830.

(104) Venable, R. M.; Luo, Y.; Gawrisch, K.; Roux, B.; Pastor, R. W. *J. Phys. Chem. B* **2013**, *117*, 10183.

(105) Venable, R. M.; Sodt, A. J.; Rogaski, B.; Rui, H.; Hatcher, E.; MacKerell, A. D., Jr; Pastor, R. W.; Klauda, J. B. *Biophys. J.* **2014**, *107*, 134.